Journal of
Materials Chemistry C

Materials for optical, magnetic and electronic devices

Accepted Manuscript

This article can be cited before page numbers have been issued, to do this please use: Y. Huang, W. luan, M. Liu and L. Turyanska, *J. Mater. Chem. C*, 2020, DOI: 10.1039/C9TC06566K.

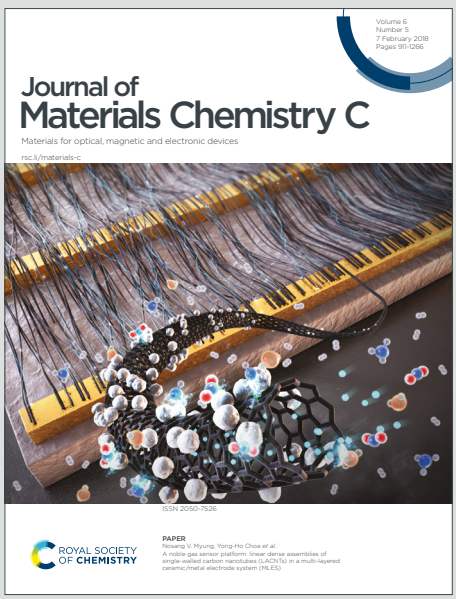

ROYAL SOCIETY OF CHEMISTRY

rsc.li/materials-c

View Article Online
DOI: 10.1039/C9TC06566K

ARTICLE

DDAB-Assisted Synthesis of Iodine-Rich $CsPbI_3$ Perovskite Nanocrystals with Improved Stability in Multiple Environments

Received 00th January 20xx,
Accepted 00th January 20xx

DOI: 10.1039/x0xx00000x

Yihui Huang,[a] Weiling Luan,*[a] Mengke Liu,[a] and Lyudmila Turyanska[b]

All-inorganic cesium lead halide perovskite ($CsPbX_3$, X = Cl, Br, I) nanocrystals (NCs) have attracted considerable attention due to their tunable optical properties and high optical quantum yield. However, their stability in various environments, such as exposure to different solvents, high temperature and UV light, remains to be addressed to enable their exploitation in devices. Here we report on synthesis of all inorganic $CsPbI_3$ perovskite nanocrystals caped with didodecyldimethylammonium bromide (DDAB). Monodispersed DDAB-capped $CsPbI_3$ NCs have enhanced stability with respect to their morphological and optical properties compared to conventional oleic acid (OA) / oleylamine (OLA) capped nanocrystals. The DDAB-$CsPbI_3$ NCs retain optical quantum yield >80 % for at least 60 days. The enhanced stability is explained by binding of branched DDAB ligands to the NC surface, leading to the formation of halogen-rich surface, as confirmed by X-ray photoelectron spectroscopy, with the iodine to lead atomic ratio of I:Pb = 4 :1. These perovskites were used in light-emitting diodes (LEDs) and had a maximum external quantum efficiency (EQE) of 1.25%, luminance of 468 cd/m^2 and demonstrated improved operational performance. The enhanced stability of DDAB-$CsPbI_3$ in the environments relevant for device processing and operation is relevant for their exploitation in optoelectronics.

Introduction

All-inorganic cesium lead halide perovskite ($CsPbX_3$, X = Cl, Br, I) nanocrystals (NCs) could offer significant advantages for applications in optoelectronic devices due to their narrow photoluminescence lines, high optical quantum efficiency and higher stability, compared with hybrid organic-inorganic perovskites.[1-4] However, their ionic nature, surface instability and the metastable structure leads to phase transition from cubic phase (α-phase) to orthorhombic phase (δ-phase) and degradation,[5-8] making them sensitive to environmental factors such as temperature, exposure to light and moisture.

To date different synthetic methods and post-synthesis modifications were proposed to improve the optical stability of these materials.[9-14] The quality of surface passivation is known to be detrimental to the stability of NCs, and to affect their optical properties.[15] Hence the choice of capping ligands is of paramount importance, with particular focus on strength of binding to the NC surface.[16] Traditionally, tri-n-octylphosphine (TOP) is used in perovskite synthesis, as organolead compound TOP-PbI_2 is an active precursor and can improve the QY and stability of perovskites.[17] To date, ammonium salts were successfully used to improve the optical properties of perovskites.[18] Environmental stability of perovskites was also addressed by selection of ligands, e.g. the use of 2-aminoethanethiol (AET) was found to enhance the stability of $CsPbI_3$ NCs in water and under ultraviolet irradiation,[19] while trimethylsilyl (TMSI) improves thermal stability (up to 130 °C).[20] Surface passivation with inorganic layers, (e.g. PbS capped nanocrystals,[21] ZnX_2/hexane[22]) and with polymers with dense network structure (e.g. poly(maleic anhydride-alt-1-octadecene) (PMA)[23]) have also been explored to enhance chemical, optical and environmental stability of NCs. However, despite a body of work, the instability of perovskites in various environments remains to be addressed.

Here we report on synthesis of all inorganic $CsPbI_3$ NCs capped with didodecyldimethylammonium bromide (DDAB). Since DDA^+ has stronger affinity to negative sites (e.g. I^-) and shorter branched chain, we expect that it will provide effective surface passivation and will facilitate transfer of photoexcited changes enabling use of these NCs in LEDs. We optimize the synthesis procedure to produce $CsPbI_3$ NCs and examine their long-term stability, thermal stability, photostability, and stability against polar solvent. The DDAB-capped $CsPbI_3$ NCs have narrow size distribution, high quantum yields up to > 90 % and are significantly more stable compared to those capped with oleic acid (OA) & oleylamine (OLA). We attribute enhanced stability to efficient passivation of the NCs by DDAB and the formation of iodine-rich surface as confirmed by our elemental analysis studies. We use these NCs in LED devices and achieve a maximum EQE and maximum luminance of 1.25% and 468 cd/m^2, respectively. The LEDs produced with DDAB-capped perovskites also show enhanced operational stability. Our synthesis method and stability studies offer an alternative strategy for achieving long term stability of perovskite nanocrystals, and are relevant for their exploitation in functional devices.

[a] Key Laboratory of Pressure Systems and Safety (MOE), School of Mechanical and Power Engineering, East China University of Science and Technology, Shanghai 200237, P.R. China. E-mail: luan@ecust.edu.cn
[b] Faculty of Engineering, University of Nottingham, University Park, NG72RD, UK.
† Electronic Supplementary Information (ESI) available: characterization data, and additional experimental procedures. See DOI: 10.1039/x0xx00000x

Experimental

Chemicals

Caesium carbonate (Cs_2CO_3, 99.9%), lead (II) iodide (PbI_2, 99%,), 1-octadecene (ODE, 90%) and poly (3,4-ethylenedioxythiophene): poly (styrenesulfonate) (PEDOT: PSS) were purchased from Adamas. Oleylamine (OLA, 80-90%) and oleic acid (OA, 85%) were purchased from Aladdin. Tmpypb, LiF, and poly (4-butyl phenyl-diphenylamine) (poly-TPD) were purchased from Xi' an Polymer Light Technology Corporation. Tri-n-octylphosphine (TOP, Tech. 90%) was purchased from Alfa and didodecyldimethylammonium bromide (DDAB, 98%) was purchased from TCI. All the reagents were used as received without any purification.

Synthesis of DDAB-capped $CsPbI_3$ NCs

To prepare Cs-oleate precursor, 0.12 g (0.36 mmol) Cs_2CO_3 and 12 mL ODE were loaded into a three-necked flack and degassed at 120 °C for 10 min under nitrogen flow. Then 0.4 mL OA and 0.4 mL OLA with 0.2 M DDAB were added. The mixture was stirred for 1 h under nitrogen flow until all Cs_2CO_3 was dissolved. The Pb-precursor solution was prepared by mixing 2.5 mL of TOP with 2 mmol of PbI_2 under stirring at 100 °C until the solution turned clear. To synthesize the $CsPbI_3$ nanocrystals, the Pb-precursor was quickly injected into Cs-oleate precursor under stirring at 160 °C. A few seconds later (5s), the solution of DDAB-$CsPbI_3$ perovskites was cooled on ice-bath.

Synthesis of OA/OLA-$CsPbI_3$ NCs

$CsPbI_3$ nanocrystals were prepared following modified method from Reference.[7] To prepare Cs-oleate precursor, 0.65 g (2 mmol) Cs_2CO_3, 2.5 mL OA and 18 mL ODE were loaded into a three-necked flask and the mixture was stirred for 1 h at 120 °C under nitrogen flow until Cs_2CO_3 was dissolved. The Pb-precursor was prepared by mixing 20 mL ODE, 2 mmol PbI_2, 3 mL OA and 3 mL OLA under stirring at 120 °C until clear solution is formed. Then the temperature of Pb-precursor was raised to 160 °C and 2 mL of Cs-oleate precursor was quickly injected under stirring. After 20 s of mixing, solution of $CsPbI_3$ perovskites was cooled on ice-bath.

Purification of perovskite nanocrystals

As-prepared crude solution of $CsPbI_3$ and DDAB-$CsPbI_3$ were centrifuged at 10000 rpm for 10 min. The precipitate was collected, dissolved in 20 mL of of n-hexane and ethylacetate (1:3 v/v), and the solution was centrifuged at 10000 rpm for 10 min. The precipitate was collected and dissolved in n-hexane (10 mL) and centrifuged for 5 min at 10000 rpm. Finally, the supernatant was collected and stored at 4 °C.

Fabrication of $CsPbI_3$ based QLEDs

The ITO glass substrate was washed in ultra-pure water, acetone and isopropyl alcohol in an ultrasonic bath, followed by treatment in UV ozone cleaning machine for 10 min. The PEDOT: PSS was spin-coated on ITO glass at 4000 rpm for 40 s and annealed at 130 °C for 15 min in air. Then a solution of TPD was spin-coated onto the PEDOT: PSS film at 3000 rpm for 40 s and annealed at 130 °C for 15min. The layer of $CsPbI_3$ was deposited by spin-coating onto the film of TPD at 1500 rpm for 40 s and heated at 40 °C for 10 min to evaporate excess hexane. The top layers of Tmpypb, LiF and Al were thermally evaporated to form the QLED.

Characterization methods

A UV-vis spectrometer (Varian Cary 50, Varian Inc.) and a fluorescence spectrophotometer (Varian Cary Eclipse, Varian Inc.) were used to measure absorption and photoluminescence of $CsPbI_3$ NCs in a quartz cell cuvette (10 mm x 10 mm) at room temperature. The time-resolved PL spectra of the $CsPbI_3$ solution was measured using Edinburgh FLS1000 spectrometer. Powder X-ray diffraction (XRD) was recorded using a Rigaka D/max2250 X-ray powder diffractometer equipped with Cu Kα radiation (λ=1.5406 Å). Transmission electron microscopy (TEM) and high-resolution TEM (HRTEM) images were collected using JEOL JEM 2100. Fourier-transformed infrared spectroscopy (FTIR) was recorded in an Aicolex Nexus470. X-ray photoelectron spectroscopy (XPS) was analyzed in a Thermo Scientific K-Alpha+. Zeta potentials were measured using Malvern Zetasizer Nano ZS 90. Luminance (*L*)-current density (*J*)-voltage (*V*) characteristics were recorded through a Keithley 2400 source.

Results and discussion

Synthesis of $CsPbI_3$ nanocrystals

We synthesize all-inorganic perovskite nanocrystals (NCs) $CsPbI_3$ capped with a mixture of OA/OLA ligands (molar ratio OA : OLA = 1 : 0.97), and with additional DDAB branched ligand (molar ratio OA : OLA : DDAB = 1 : 0.97 : 0.06) (Figure 1a). These $CsPbI_3$ and DDAB-$CsPbI_3$ NCs have optical emission centered at 680 nm and 685 nm, respectively. As-synthesized DDAB-$CsPbI_3$ NCs have narrower linewidth (FWHM = 95 meV), and ~15% higher optical quantum yield (QY) of 95%, compared to OA/OLA capped NCs (Figure 1b). The radiative recombination time is also increased for DDAB-capped NCs (inset in Figure 1b), suggesting lower density of surface defects. The TEM studies reveal the cubic shape of the NCs with an average size of 11.9±2.4 nm for OA/OLA-$CsPbI_3$ and 13.7±2.3 nm for DDAB-$CsPbI_3$. The observed larger size for DDAB-$CsPbI_3$ NCs is consistent with the use of TOP in their synthesis, which increases precursor activity accelerating the growth of NCs.[17, 24] Presence of DDAB ligands provides more efficient passivation of the surface and reduces amount of surface defects, as evident from smaller size and high QY, compared with NCs only prepared by TOP (Figure 2a, and Supplementary Information, Figure S2).

To optimize the synthesis procedure, we examined the effect of DDAB amount on the optical properties of NCs. With increasing DDAB concentration from 0 M to 0.3 M, we observe broadening of the optical line by ~15 meV and a blueshift of PL emission from 691 nm to 677 nm (Figure 2a). The optical QY and nanocrystal shelf life were also affected by the DDAB concentration: for NCs synthesised

with 0.2M DDAB, we observed the highest value of QY = 95% (Figure 2a) and long shelf life (Figure S1c). Our TEM studies show that with increasing amount of DDAB, the average size of the NCs decreases from 17.5±2.2 nm to 12.9±2.1 nm (Figure 2b and Figure S2). Since XPS and EDX studies do not reveal measurable amount of Br, we envisage that the observed blueshift of PL is due to the size decrease. It is known that the stability and optical properties of the perovskites depend on the type of crystal lattice. Our X-ray diffraction (XRD) measurements revealed that all DDAB capped samples have interplanar distances of 0.62 nm, corresponding to (100) plane of cubic phase (Figure 2c). Crystal lattice spacing of 0.62 nm is also observed in HR TEM images, confirming the XRD results (Figure 3c, d).

Optical stability in different environment

Since the NCs with 0.2M DDAB have the highest value of QY = 95% and longest shelf life, we use them for further studies. To assess the stability of $CsPbI_3$ NCs synthesized with 0.2 M DDAB, their optical properties were continuously monitored over two months period. Stored in the dark, the DDAB-capped NCs maintained stable photoluminescence properties, with QY > 80%. In contrast, the QY of OA/OLA-capped $CsPbI_3$ NCs decreased dramatically after 10 days, with measured QY < 20% (Figure 3a). Changes in optical properties are also accompanied by changes in morphology of the NCs. The XRD measurements confirm stable cubic phase for DDAB capped perovskites and degradation of OA-OLA-capped nanocrystals to orthorhombic phase (Figure 3b). As-synthesized NCs have cubic shape and average sizes of 11.9±2.4 nm and 13.7±2.3 nm for OA/OLA and DDAB-capped $CsPbI_3$ NCs, respectively. However, following 30-day storage, we observe aggregation of OA/OLA capped nanocrystals into large nanorods with length of ~1 µm (Figure 3c). For the DDAB- $CsPbI_3$ NCs, we do not observe any significant changes in the NC shape and size over 60-day study (Figure 3d). The DDAB-$CsPbI_3$ NCs retain narrow size distribution and no phase transformation is observed.

It is known that OLA ligands are commonly used for surface passivation for the perovskite NCs,[25-26] however, any excess of OLA could hinder nucleation and cause NCs to degradation.[27-28] In our synthesis, we use reduced amount of OLA compared to reported values[20] to ensure no ligand excess is present in the mixture. The binding of the OA and OLA ligands to the NC surface is weak and loss of ligands leads to formation of surface defects, such as halogen vacancies, resulting in decrease of PL QY and gradual agglomeration of the NCs.[29-30] The long term stability of our DDAB capped NCs indicates that DDAB ligands provide efficient binding and enhance the perovskite optical and phase stability.

Fourier-transform infrared spectroscopy (FTIR) was performed to analyse ligand attachment to the NCs surface. As can be seen from Figure 4a, the spectrum of OA/OLA-$CsPbI_3$ NCs reveals broad resonances centred at 3323cm^{-1}, corresponding to stretching vibrations of ammonium group (ν(N-H_3^+)).[31] For the DDAB-$CsPbI_3$ sample, this resonance is not detectable, indicating that the addition of DDAB into the ligand mixture leads to ligand replacement on the NC surface and/or preferential binding of DDAB

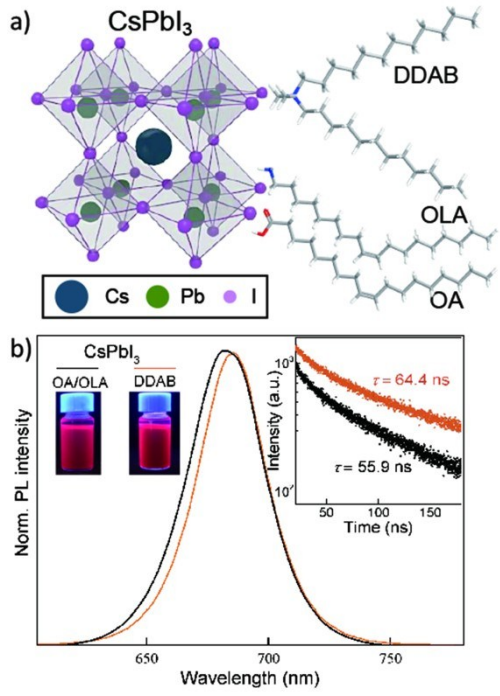

Fig. 1 (a) The structure of DDAB-$CsPbI_3$ NCs and OA/OLA $CsPbI_3$ NCs. (b) Room temperature PL spectra, (left inset) photographs and (right inset) time-resolved PL of DDAB-$CsPbI_3$ NCs and OA/OLA $CsPbI_3$ NC solutions.

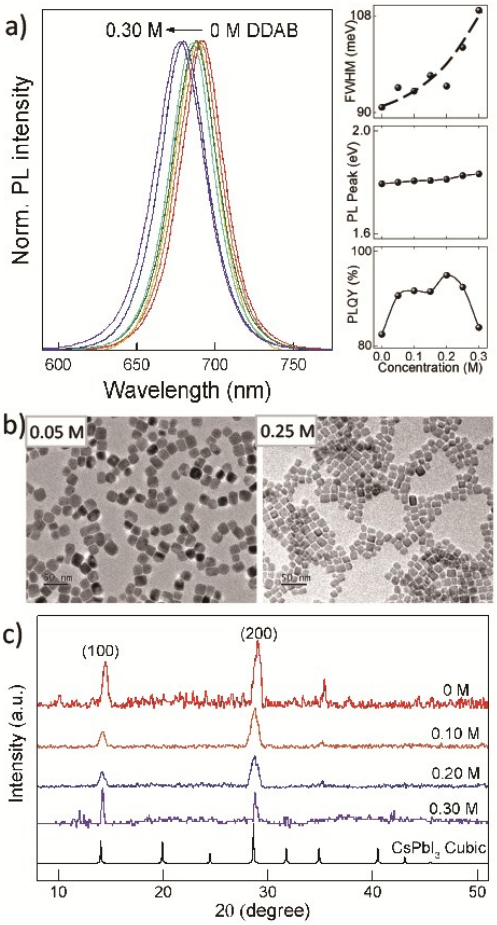

Fig. 2 (a) The blue shift of PL spectra of $CsPbI_3$ NCs obtained by different concentration of DDAB. Inset in (a) are the variation of optical properties of $CsPbI_3$ NCs obtained by different concentration of DDAB. (b) TEM images of $CsPbI_3$ NCs prepared by 0.05 M DDAB and 0.25 M DDAB on the first day. (c) XRD patterns of $CsPbI_3$ NCs films obtained by different concentration of DDAB.

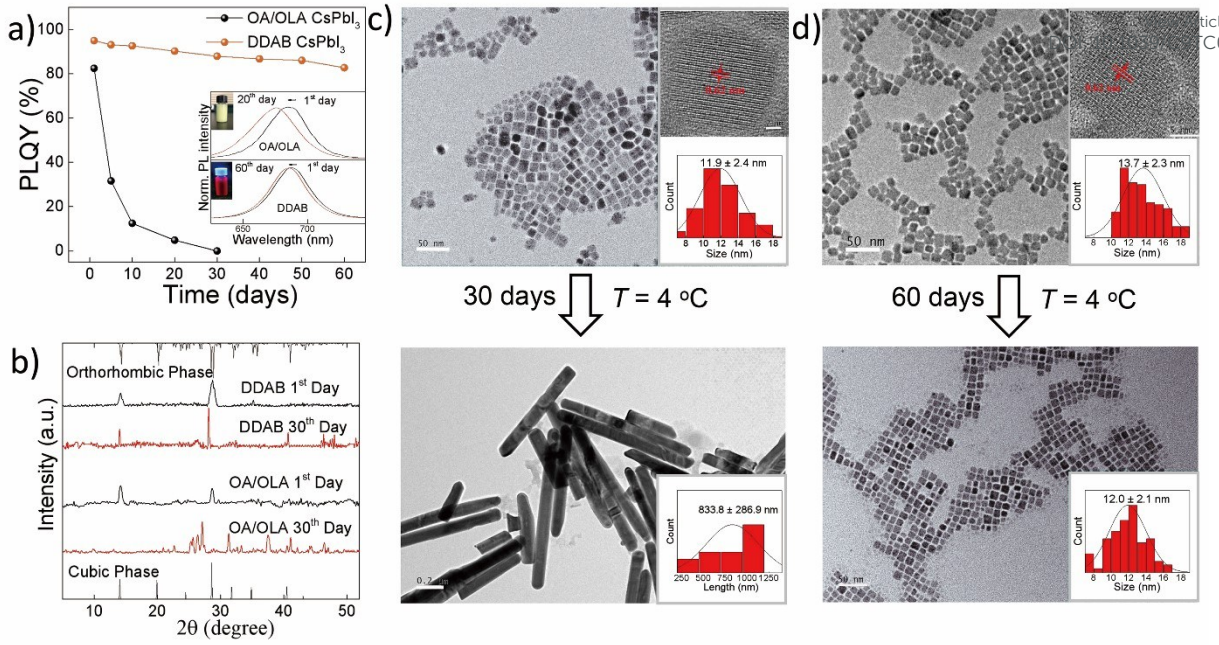

Fig.3 (a) PLQY of OA/OLA $CsPbI_3$ NCs and DDAB-$CsPbI_3$ NCs as a function of storage time. Insert in (a) is the variation of PL peak in different periods (b) XRD patterns of $CsPbI_3$ NCs films on the first day and the 30th day. TEM and HRTEM images of (c) OA/OLA $CsPbI_3$ NCs on the first day and the 30th day, and (d) DDAB-$CsPbI_3$ NCs on the first day and the 60th day. Inset in (c) and (d) are the corresponding particle size distribution.

over OA/OLA ligands. To further probe the composition of the ligand layer, we performed X-ray photoelectron spectroscopy. We observe comparable intensity of Cs 3d and Pb 4f resonances for both samples (Figure S4a-c), however an increase in the intensity of I 3d is observed for DDAB-capped NCs. We estimate the atomic ratio of I : Pb to be 4 : 1 for DDAB- and 3 : 1 for OA/OLA-capped NCs (Figure 4b). The high-resolution XPS spectra of the N 1S also reveal noticeable differences (Figure S4d,e): for OA/OLA-$CsPbI_3$ NCs, the N 1S spectrum can be fitted into two peaks at 399.9 eV and 401.8 eV, representing $-NH_2$ and $-NH_3^+$; for DDAB-$CsPbI_3$ we also observe a

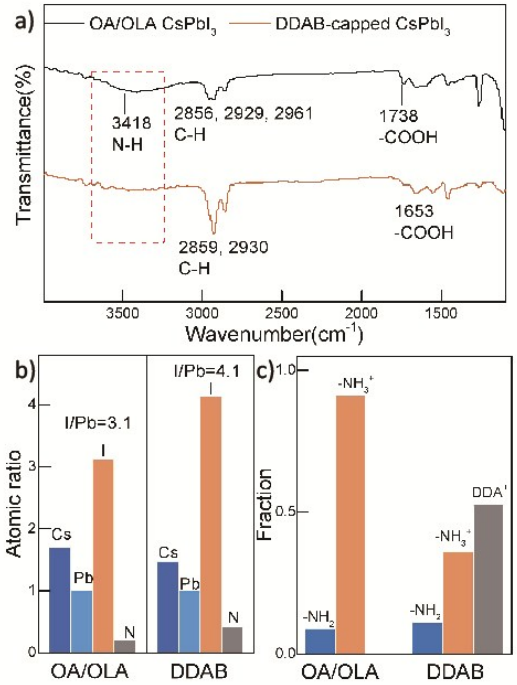

Fig. 4 (a) FTIR, (b) the atomic ratio, (c) the ratio of $-NH_2$, $-NH_3^+$, and DDA^+ of OA/OLA $CsPbI_3$ NCs and DDAB-$CsPbI_3$ NCs.

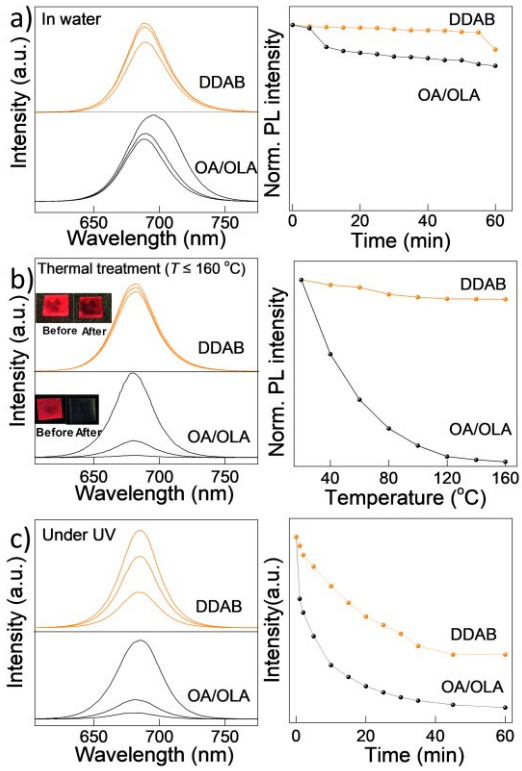

Fig. 5 PL emission spectra and the PL intensity change of OA/OLA $CsPbI_3$ and DDAB-$CsPbI_3$ NCs (a) solutions in water, (b) films under different temperature, (c) solutions under UV radiation (365 nm).

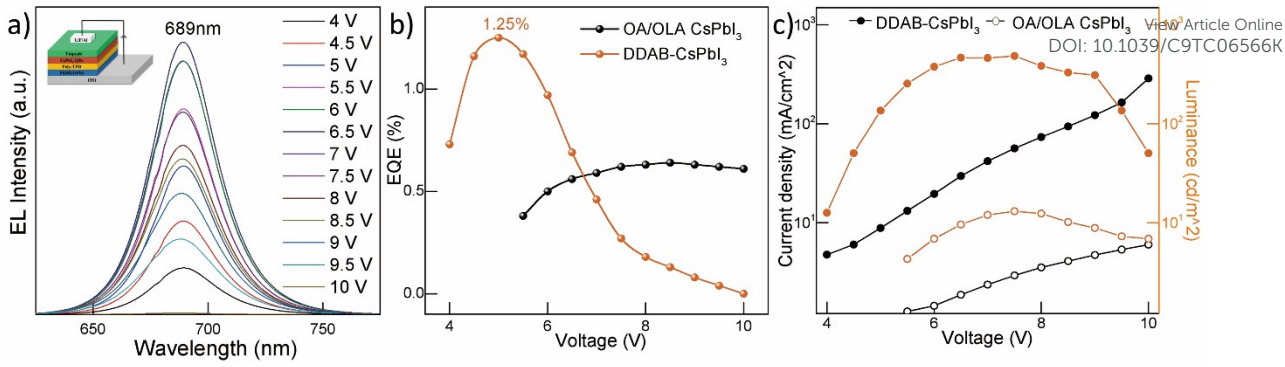

Fig.6 (a) Electroluminescence (EL) spectra of LED based on DDAB-$CsPbI_3$ NCs under different voltage. Insert in (a) is the device structure of $CsPbI_3$ LED. (b) EQE and (c) current density and luminance of LEDs based on DDAB-$CsPbI_3$ NCs and OA/OLA $CsPbI^3$ NCs as a function of voltage.

peak at 402.2 eV corresponding to tert-ammonium cations from DDA^+ cations.[32-33] Analysis of the ratio of these functional groups reveals that the increase of the fraction of DDA^+ is accompanied by a decrease in -NH_3^+ (Figure 4c), thus confirming that DDAB replaces OLA on the NC surface.

Our XPS results show that the addition of the DDAB ligands leads to the formation of I-rich NCs. We envisage that I-rich negatively charge NC surface provides a strong binding to the DDA^+. Surface defects in NCs are predominantly atomic vacancies, which act as nonradiative recombination centers and lead to reduced PL QY.[34] In perovskite NCs, the halogen vacancies dominate surface properties of all-inorganic NCs,[35] hence we attribute enhanced long term optical stability of DDAB capped perovskites to the formation of halogen-rich $CsPbI_3$ NCs with reduced density of halogen vacancies. Our zeta-potential measurements confirm that DDAB-$CsPbI_3$ NCs have I-rich surface as we observed more negative surface potential of -36.3 mV for DDAB-$CsPbI_3$ NCs, compared to -25 mV for OA/OLA-$CsPbI_3$ NCs. The combination of more negative surface potential and branched structure of DDAB providing steric hindrance is beneficial for long term colloidal stability of the NCs.

Highly ionic nature of perovskites makes them highly susceptible to environmental factors, such as humidity, temperature, and ultraviolet radiation.[36] Therefore, we assess the stability of optical properties on the NCs following exposure to polar solvents (water and ethanol), UV illumination and increased temperature. As seen in Figure 5a, DDAB-$CsPbI_3$ is significantly more stable in water with <5% loss in PL intensity over 50 min exposure. To evaluate the thermal stability, the NCs were spin-coated on ITO glass and heated from 20 °C to 160 °C (Figure 5b). The PL intensity of OA/OLA-$CsPbI_3$ film decreased by 93% and the film became yellow indicating phase transformation. Thermal stability of DDAB-$CsPbI_3$ NCs is significantly improved, with only ~11% decrease of PL intensity observed. Similar increase in stability is observed under UV exposure (Figure 5c): the PL intensity of OA/OLA-$CsPbI_3$ decreased drastically with no detectable emission observed after 1 hour exposure, which can be attributed to photooxidation process resulting in the aggregation of NCs[37]. At the same condition, the DDAB-$CsPbI_3$ maintains ~47% of the original PL intensity. We attribute the improved thermal stability and photostability to stronger binding and I-rich surface in DDAB-$CsPbI_3$ NCs, which increases the resistance environment-induced phase transition.

Light-emitting diodes

Enhanced environmental stability of the DDAB-$CsPbI_3$ NCs makes them promising candidates for device applications. To confirm that enhanced stability of the NCs can be used to enhance the operational stability of devices, we use DDAB- $CsPbI_3$ to fabricate QLEDs (inset in Figure 6a). The QLED consists of multiple layers: indium tin oxide glass substrate, poly (3,4-ethylenedioxythiophene): poly (styrenesulfonate) (PEDOT: PSS) (hole-injection layer), poly (4-butylphenyl-diphenylamine) (poly-TPD) (hole-transporting layer), DDAB-$CsPbI_3$ (0.2 M DDAB), Tmpypb (electron-transporting layer). The fabricated QLEDs emit red light with a peak centred at 689 nm and a narrow linewidth, FWHM = 36 nm (Figure 6a). We observe a small redshift of EL peak compared to the PL peak position, due to Stark effect.[38] The comparison of device performance of QLED with a layer of DDAB-$CsPbI_3$ and OA/OLA-$CsPbI_3$ NCs is shown in Figure 6b-c. Higher current density is observed for LEDs based on DDAB-$CsPbI_3$, indicating better carrier injection and transport ability. This enhancement is related to lower density of surface defects and more efficient passivation of dangling bonds on the NCs by DDAB ligands. The turn-on voltage for DDAB-$CsPbI_3$ NCs is also lower (4 V) and maximum EQE is ~2 times higher (1.25 %) compared to OA/OLA-$CsPbI_3$ (5.5 V). The luminance of DDAB-NCs is ~100 times improved (at V = 6 V), confirming advantages of our DDAB-capped NCs for device application. To fabricate efficient optoelectronic devices, perovskite NCs should have high optical quantum yield and should enable effective transfer of photoexcite changes into a change transporting layer. Our feasibility studies demonstrate that DDAB-capped nanocrystals can be advantageous for long term stability of LEDs, however further studies are needed to enhance the device performance and can be achieved by optimization of the device architecture to improve charge transfer.

Conclusions

We developed and optimised a method to synthesis iodine-rich $CsPbI_3$ NCs with enhanced environmental stability (polar solvents, temperature up to 160 °C and long-term UV illumination). The use of DDAB as a ligand provides strong binding to the NC surface and efficient passivation of the surface defects which leads to long-term stability of optical properties and high PL quantum yields >80% for at least 60 days. We demonstrated that the achieved enhanced optical, phase and environmental stability of the NCs is translated into enhanced operational performance of the QLEDs based on DDAB- $CsPbI_3$. Our results are transferable to other perovskite

NCs and are relevant for their implementation of different optoelectronic devices.

Conflicts of interest

There are no conflicts to declare.

Acknowledgements

The work was supported by East China University of Science and Technology. Authors acknowledge useful discussions and technical support from the staff at the Analysing&Testing Center of East China University of Science and Technology.

Notes and references

1 M. Lu, Y. Zhang, S. Wang, J. Guo, W. Yu, and A.L. Rogach, *Adv. Funct. Mater.*, 2019, **29**, DOI: 10.1002/adfm.201902008.
2 M. Jung, S. G. Ji, G. Kim, and S. -I. Seok, *Chem. Soc. Rev.,* 2019, **48**, 2011-2038.
3 D. Yang, M. Cao, Q. Zhong, P. Li, X. Zhang and Q. Zhang, *J. Mater. Chem. C,* 2019, **4**, 757-789.
4 L. Jiang, Z. Fang, H. Lou, C. Lin, Z. Chen, J. Li, H. He, and Z. Ye, *Phys. Chem. Chem. Phys.,* 2019, **21**, 21996-22001.
5 V. Nandal, and P. Nair, *ACS Nano,* 2017, **11**, 11505-11512.
6 H. Huang, M. I. Bodnarchuk, S. V. Kershaw, M. V. Kovalenko, and A. L. Rogach, *ACS Energy Lett.,* 2017, **2**, 2071-2083.
7 A. Swarnkar, W. J. Mir, and A. Nag, *ACS Energy Lett.,* 2018, **3**, 286-289.
8 J. Sun, S. Huang, X. Liu, Q. Xu, Q. Zhang, W. Jiang, D. Xue, J. Xu, J. Ma, J. Ding, Q. Ge, L. Gu, X. Fang, H. Zhong, J. Hu, and L. Wan, *J. Am. Chem. Soc.,* 2018, **140**, 11705-11715.
9 L. Protesescu, S. Yakunin, M. I. Bodnarchuk, F. Krieg, R. Caputo, C. H. Hendon, R. X. Yang, A. Walsh, and M. V. Kovalenko, *Nano Lett.,* 2015, **15**, 3692-3696.
10 Q. A. Akkerman, V. Dinnocenzo, S. Accornero, A. Scarpellini, A. Petrozza, M. Prato, and L. Manna, *J. Am. Chem. Soc.,* 2015, **137**, 10276-10281.
11 C. Zhang, W. Luan, Y. Yin, F. Yang, *Beilstein J Nanotechnol.,* 2017, **8**, 2521-2529.
12 Y. Li, H. Huang, Y. Xiong, S. V. Kershaw, and A. L. Rogach, *Angew. Chem. Int. Ed. Engl.,* 2018, **57**, 5833-5837.
13 X. Fu, C. Zhang, Z. Peng, Y. Xia, J. Zhang, W. Luo, R. Zhan, H. Li, Y. Wang and D. Zhan, *J. Mater. Chem. C,* 2018, **6**, 1701-1708.
14 L. Wu, Q. Zhong, D. Yang, M. Chen, H. Hu, Q. Pan, H. Liu, M. Cao, Y. Xu, B. Sun, and Q. Zhang, *Langmuir,* 2017, **33**, 12689-12696.
15 J. De Roo, I. Van Driessche, J. C. Martins, and Z. Hens, *Nat. Mater.,* 2016, **15**, 517-521.
16 J. De Roo, M. Ibáñez, P. Geiregat, G. Nedelcu, W. Walravens, J. Maes, J. C. Martins, I. Van Driessche, M. V. Kovalenko, and Z. Hens, *ACS Nano,* 2016, **10**, 2071-2081.
17 F. Liu, Y. Zhang, C. Ding, S. Kobayashi, T. Izuishi, N. Nakazawa, T. Toyoda, T. Ohta, S. Hayase, T. Minemoto, K. Yoshino, S. Dai, and Q. Shen, *ACS Nano,* 2017, **11**, 10373-10383.
18 R. L. Z. Hoye, M. Lai, M. Anaya, Y. Tong, K. Galkowski, T. Doherty, W. Li, T. N. Huq, S. Mackowski, L. Polavarapu, J. Feldmann, J. L. MacManus-Driscoll, R. H. Friend, A. S. Urban, S. D. Stranks, *ACS Energy Lett.,* 2019, **4**, 1181-1188.
19 C. Bi, S. V. Kershaw, A. L. Rogach, and J. Tian, *Adv. Funct. Mater.,* 2019, **29**, DOI: 10.1002/adfm.201902446.
20 Y. Cai, H. Wang, Y. Li, L. Wang, Y. Lv, X. Yang, and R. Xie, *Chem. Mater.,* 2019, **31**, 881-889.
21 X. Zhang, M. Lu, Y. Zhang, H. Wu, X. Shen, W. Zhang, W. Zheng, V. L. Colvin, W. W. Yu, *ACS Cent. Sci.,* 2018, **4**, 1352-1359.
22 F. Li, Y. Liu, H. Wang, Q. Zhan, Q. Liu, Z. Xia, *Chem. Mater.,* 2018, **30**, 8546-8554.
23 M. Meyns, M. Peralvarez, A. Heuer-Jungemann, W. Hertog, M. Ibanez, R. Nafria, A. Genc, J. Arbiol, M. V. Kovalenko, J. Carreras, A. Cabot, A. G. Kanaras, *ACS Appl. Mater. Interfaces,* 2016, **8**, 19579-19586.
24 H. Wang, N. Sui, X. Bai, Y. Zhang, Q. Rice, F. J. Seo, Q. Zhang, V. L. Colvin, and W. Yu, *J. Phys. Chem. Lett.,* 2018, **9**, 4166-4173.
25 A. Pan, B. He, X. Fan, Z. Liu, J. J. Urban, A. P. Alivisatos, L. He, and Y. Liu, *ACS Nano,* 2016, **10**, 7943-7954.
26 J. Kang, and L. Wang, *J. Phys. Chem. Lett.,* 2017, **8**, 489-493.
27 S. Seth, and A. Samanta, *Sci. Rep.,* 2016, **6**, DOI: 10.1038/srep37693.
28 E. Yassitepe, Z. Yang, O. Voznyy, Y. Kim, G. Walters, J. A. Castañeda, P. Kanjanaboos, M. Yuan, X. Gong, F. Fan, J. Pan, S. Hoogland, R. Comin, O. M. Bakr, L. A. Padilha, A.F. Nogueira, and E. H. Sargent, *Adv. Funct. Mater.,* 2016, **26**, 8757-8763.
29 T. Udayabhaskararao, M. Kazes, O. Houben, H. Lin, and D. Oron, *Chem. Mater.,* 2017, **29**, 1302-1308.
30 F. Krieg, S. T. Ochsenbein, S. Yakunin, S. Ten Brinck, P. Aellen, A. Süess, B. Clerc, D. Guggisberg, O. Nazarenko, Y. Shynkarenko, S. Kumar, C.-J. Shih, I. Infante, and M. V. Kovalenko, *ACS Energy Lett.,* 2018, **3**, 641-646.
31 M. Chong, and X. Zhao, *Phys. Chem. B.,* 2003, **107**, 12650-12657.
32 M. S. Bakshi, S. Sachar, G. Kaur, P. Bhandari, G. Kaur, M.C. Biesinger, F. Possmayer, and N. O. Petersen, *Cryst. Growth Des.* 2008, **8**, 1713-1719.
33 J. Pan, L. Quan, Y. Zhao, W. Peng, B. Murali, S. P. Sarmah, M. Yuan, L. Sinatra, N. M. Alyami, J. Liu, E. Yassitepe, Z. Yang, O. Voznyy, R. Comin, M. N. Hedhili, O. F. Mohammed, Z. Lu, D. Kim, E. H. Sargent, and O. M. Bakr, *Adv. Mater.,* 2016, **28**, 8718-8725.
34 D. V. Talapin, J. Lee, M. V. Kovalenko, and E. V. Shevchenko, *Chem. Rev.,* 2010, **110**, 389-458.
35 S. Seth, T. Ahmed, A. De, and A. Samanta, *ACS Energy Lett.,* 2019, **4**, 1610-1618.
36 Y. Reyna, A. Pérez-Tomás, A. Mingorance, M. Lira-Cantú. in Molecular Devices for Solar Energy Conversion and Storage, ed. H. Tian, G. Boschloo, A. Hagfeldt, Springer, Singapore, 2018, 477-531.
37 X. Li, F. Cao, D. Yu, J. Chen, Z. Sun, Y. Shen, Y. Zhu, L. Wang, Y. Wei, Y. Wu, H. Zeng, Small, 2017, **13**, DOI:10.1002/smll.201603996.
38 J. Pan, Y. Shang, J. Yin, M. De Bastiani, W. Peng, I. Dursun, L. Sinatra, A. M. El-Zohry, M. N. Hedhili, A. H. Emwas, O. F. Mohammed, Z. Ning, and O. M. Bakr, *J. Am. Chem. Soc.,* 2018, **250**, 562-565.

View Article Online
DOI: 10.1039/C9TC06566K

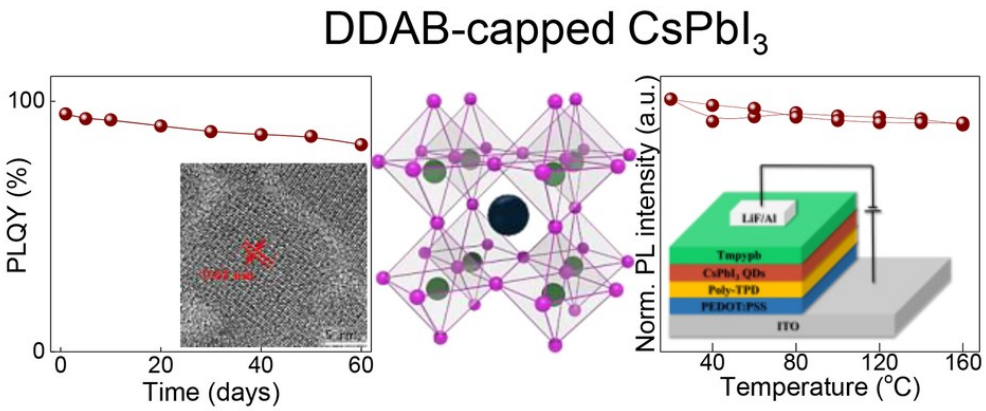

80x32mm (300 x 300 DPI)